Plasma electrolytic oxidation of aluminium in electrolytes containing various concentrations of carbon black nanoparticles

L. Magniez, C. da Silva Tousch, Sébastien Fontana, S. Cahen, J. Martin, C. Hérold, G. Henrion

Plasma electrolytic oxidation of aluminium in electrolytes containing various concentrations of carbon black nanoparticles

L. Magniez[1], C. Da Silva Tousch[1], S. Fontana[1], S. Cahen[1], J. Martin[1,2], C. Hérold[1], G. Henrion[1, 2, *]

[1] Université de Lorraine, CNRS, Institut Jean Lamour, F-54000 Nancy, France

[2] Université de Lorraine, Laboratoire d'Excellence Design of Alloy Metals for low-mAss Structures ('LabEx DAMAS'), F-57045 Metz, France

*Corresponding author: gerard.henrion@univ-lorraine.fr (G. Henrion) ; (+33) 372 742 489

Abstract

Incorporation of carbon-based nanoparticles into ceramic coatings during plasma electrolytic oxidation (PEO) is promising for the synthesis of new composite layers on lightweight metals. Specifically, the present study focuses on the incorporation of carbon black (CB) nanoparticles into PEO alumina layers. For this purpose, PEO of aluminium is performed in silicate-based electrolytes containing various concentrations of dispersed carbon black nanoparticles (from 0 to 6 $g \cdot L^{-1}$). The influence of this concentration on the microstructure of the achieved PEO coatings is investigated by combining complementary characterization techniques (scanning electron microscopy, X-ray diffraction and Raman spectroscopy). Results show that using concentrations up to 6 $g \cdot L^{-1}$ tend to limit the morphological inhomogeneity between the edges and the centre of the treated samples. Moreover, the addition of carbon black nanoparticles results in a sponge-like outermost sublayer covering larger areas of the surface with abilities to host a higher amount of these nanoparticles. It is also evidenced that CB nanoparticles do not suffer any further structural degradation during their incorporation. In addition, cross-checked results show that the presence of dispersed CB nanoparticles slightly affect the coating average growth rate. As for potential future applications, the electrical volume conductivity of grown carbon-alumina composite coatings is also measured.

Keywords: Plasma Electrolytic Oxidation (PEO); Aluminium; Alumina coating; Carbon black; Nanoparticle; Electrical volume conductivity

1. Introduction

Over the last 25 years, plasma electrolytic oxidation (PEO) also known as micro-arc oxidation (MAO) has been widely studied due to its high potential to advantageously replace anodizing that often uses hazardous chemical compounds and requires several steps of cleaning, oxidation and sealing. Moreover, PEO makes it possible to grow thick and protective oxide coatings on valve metals (*e.g.* Al, Ti; Mg, Zr) in a single step and using a non-hazardous alkaline electrolyte [1-6]. More recently, PEO has gained a new interest by considering the possibility to elaborate ceramic-based composite coatings by incorporating elements dissolved or dispersed in the electrolyte into the inherent porosity of the PEO layers.

Indeed, it seems fairly obvious that the network of pores represents privileged sites in which particles added to the electrolyte can be trapped [7-13].

The mechanisms of incorporation of particles into the PEO coating are still unclear. Some authors, however, suggest that the insertion of particles into the layers takes place according to two mechanisms that can occur either separately or simultaneously:

(i) the transport of the particles from the electrolyte to the electrode and through the extreme surface porosity under the effect of the electric field (electrophoresis). This transport is predominant during the anodic phase, especially for particles with a negative zeta potential [8, 13, 14], and

(ii) the deposition and trapping of particles on the inner walls of pores mainly driven by the electrolyte infiltration [7, 15].

According to these mechanisms, it appears that several factors can influence the insertion of particles in the PEO layers:

- their electrokinetic potential. In most cases, particles exhibit a negative zeta potential in an alkaline medium, and this potential increases in absolute value with the increase in electrolyte pH [16];
- the relative size and shape of particles and pores [7, 17];
- the composition of the electrolyte, keeping in mind that the addition of particles in the electrolyte can modify its conductivity [18-20];
- the electrical parameters of the process (applied voltage and current waveforms), which define the electric field during the anodic and/or cathodic phases as well as the micro-discharge characteristics and behaviour;
- the nature and concentration of particles dispersed in the electrolyte.

Finally, the incorporation of particles or elements from the electrolytic bath can be either inert – the particles are simply trapped in the available pores, like physisorption – or reactive. In the latter case, the incorporated elements react with the host sites and their environment, which can result in modifications of the microstructure and/or the composition of the layers [21, 22]. Depending on the desired properties of the PEO coatings, there is a wide range of particles that can be dispersed into the electrolyte and incorporated in the PEO layers. These particles include metals, ceramics, nitrides, sulfides, polymers [9, 10, 21, 23-26]. The review paper by Lu *et al.* [8] gives an extensive overview of the most used particles to improve the PEO coating properties.

Despite the large number of papers reporting on the PEO with particle incorporation, those dealing with the incorporation of carbon-based nanoparticles only account for less than 8% [27]. Moreover, most of these papers focus on the final properties of the composite coatings and only few relate to the process itself and the mechanisms of incorporation of particles during PEO.

Carbon black (CB) nanoparticles have been widely used for many decades for various applications [28], essentially as a pigment and reinforcing phase in the tire industry. Due to their electrical properties, carbon blacks are also used in various kinds of batteries [29-31] and can be incorporated in polymer matrix to elaborate conductive carbon-polymer composites [32, 33]. Hence, the present work focuses on the incorporation of carbon black nanoparticles in the PEO coatings by dispersing CB with various concentrations in the electrolyte, and on their influence on the characteristics of the resulting coatings, including the electrical volume conductivity.

2. Material and methods

2.1 Experimental set up

The PEO treatments were carried out in a 2 L beaker filled with the electrolyte containing a carbon black suspension (Fig. 1). The choice of working with a small volume tank was motivated by the presence of carbon nanoparticles. Indeed, a small volume reduces the required quantity of particles, thus reducing their consumption as well as waste by-products. Moreover, thermal regulation of the electrolyte usually involves circulating it through a heat exchanger with a pump, which is not suitable when solid particles are dispersed in the electrolyte. Indeed the particles could accumulate in the recirculation pipes and heat exchanger with the risk of clogging it. Particles could also be lost at the internal walls of the pipes and heat exchanger resulting in a decreasing particle concentration in the electrolyte during the process. Instead, cold water at a temperature of 18 °C flowed in a cooling copper coil that surrounded the electrodes, thus keeping the electrolyte temperature around 40 °C. Rectangular samples (32 × 50 × 5 mm^3 in size) made of Al-1050 (Table 1) were used as working electrodes. The processed aluminium sample and two titanium counter electrodes

(120 × 50 × 1 mm^3) were immersed in the electrolyte. The distance between the working electrode and each counter electrode was set at 20 mm. During the PEO treatment, a magnetic stirrer was used to prevent the CB nanoparticles sedimentation, and to ensure a homogeneous electrolyte temperature.

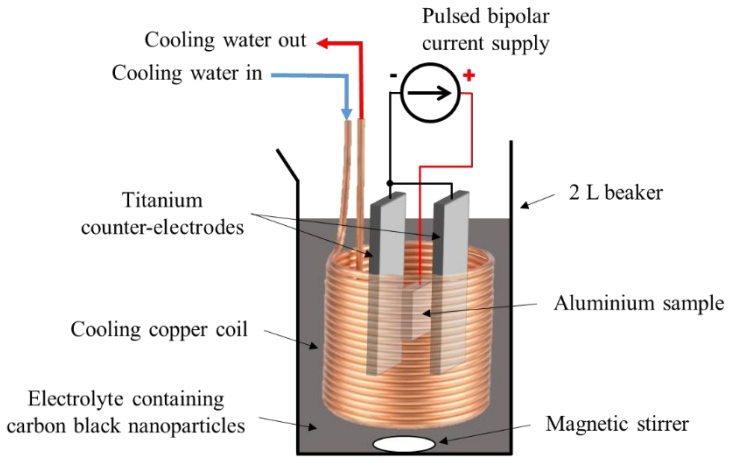

Fig. 1. Experimental setup for PEO treatments with dispersed carbon black nanoparticles in the electrolyte.

Table 1
Elemental composition of the 1050 aluminium substrate.

Element	Fe, Ti, Zn	Si	Cu	Mg	Mn	Al
wt.%	< 0.5	< 0.25	0.05	< 0.05	< 0.05	Balance

The aluminium sample and the counter electrodes were connected to a pulsed bipolar current supply (Ceratronic© CER004 [34]). The anodic and cathodic current waveforms could be adjusted in amplitude and duration to set the positive and negative charge quantity at the desired values. In the present work, the current parameters were set according to Table 2; a schematic drawing of the current waveform is depicted in Fig. 2. A full description of the current waveform is given in [35]. Within this set of parameters, the negative to positive

charge quantity ratio was slightly lower than 1 (~ 0.88), which favoured the occurrence of the "soft" sparking regime [35-37].

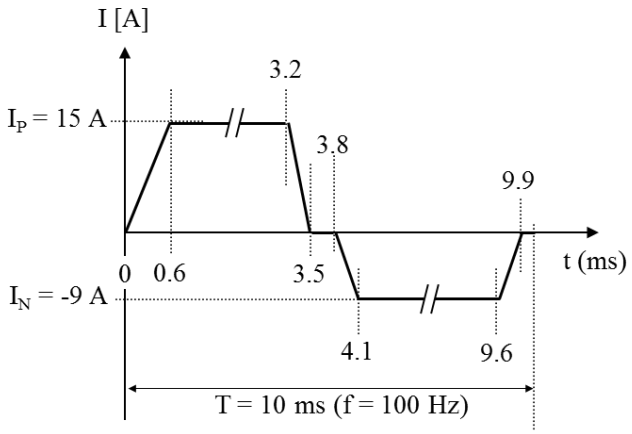

Fig. 2. Schematic drawing of one period of the current waveform indicating the time at each change in the current rising/falling rate according to Table 2.

Table 2

Parameters of the current waveform.

Current pulse frequency (Hz)		100
Anodic current pulse	Rise time (ms)	0.6
	Pulse duration (ms)	2.6
	Fall time (ms)	0.3
	Amplitude (A)	15
	Charge per pulse (C)	0.046
Delay between anodic and cathodic pulses (ms)		0.3
Cathodic current pulse	Rise time (ms)	0.3
	Pulse duration (ms)	5.5
	Fall time (ms)	0.3
	Amplitude (A)	-9
	Charge per pulse (C)	0.052

Delay between cathodic and anodic pulses (ms)	0.1

An alkaline mother solution was prepared by diluting potassium hydroxide (KOH: 1 $g \cdot L^{-1} \cong 17.86$ $mmol \cdot L^{-1}$) and sodium silicate (Na_2SiO_3: 1.65 $g \cdot L^{-1} \cong 13.52$ $mmol \cdot L^{-1}$) in deionized water. Its measured electrical conductivity and pH were 7.5 $mS \cdot cm^{-1}$ and 12.3, respectively. From this mother solution, different electrolytes were prepared by dispersing carbon black nanoparticles with concentrations ranging from 0 $g \cdot L^{-1}$ to 6 $g \cdot L^{-1}$. The carbon-based nanoparticles being intrinsically hydrophobic, the CB suspensions were submitted to probe sonication during 30 min before PEO processing. During PEO processing, both the magnetic stirrer and the electrolyte bubbling maintained the carbon nanoparticle suspension. In the following, samples are referred to as CBx, where x stands for the CB concentration (in $g \cdot L^{-1}$) in the base electrolyte as reported in Table 3. In order to avoid the ageing effect of the electrolyte [38], and to ensure a controlled CB concentration, a fresh CB suspension was made for each sample. The treatment duration was set to 60 min for each sample.

Table 3

Concentration of dispersed carbon black nanoparticles used in different electrolytes, and corresponding sample identification.

CB ($g \cdot L^{-1}$)	0	1	2	4	6
Sample name	CB0	CB1	CB2	CB4	CB6

Carbon black nanoparticles (Vulcan XC-72) were provided by Cabot Corp.

Thermogravimetric analysis (TGA Setsys Evolution 1750 Setaram) of carbon black

nanoparticles was performed prior to their dispersion in the electrolyte. The CB powder was heated in a platinum crucible under dry air from ambient temperature to 1000 °C with 3 °C min^{-1} heating rate. TGA revealed that CB nanoparticles were of high purity (less than 0.7 wt% impurities). Scanning electron microscopy (SEM FEI Quanta 650 FEG), transmission electron microscopy (TEM Phillips CM200), and Raman spectroscopy with an exciting radiation wavelength of 532 nm in the range 800-2000 cm^{-1} (Horiba Jobin-Yvon LabRam HR800) were used to characterize the produced PEO coatings as well as the as-received CB nanoparticles. SEM and TEM micrographs and the Raman spectrum of the pristine CB nanoparticles are shown in Fig. 3 and Fig. 4, respectively.

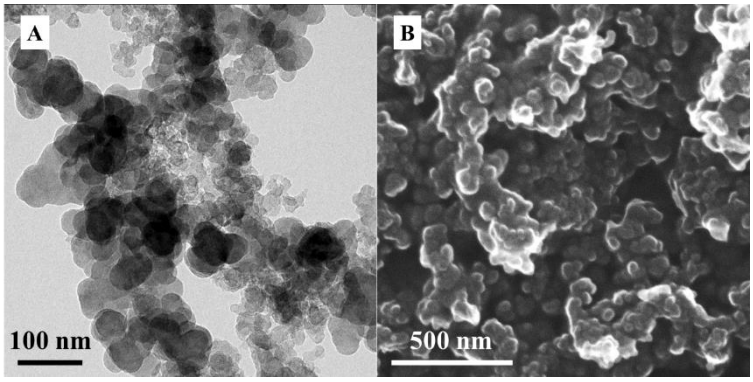

Fig. 3. TEM (A) and SEM (B) micrographs of the pristine carbon black nanoparticles used for dispersion in the PEO electrolyte.

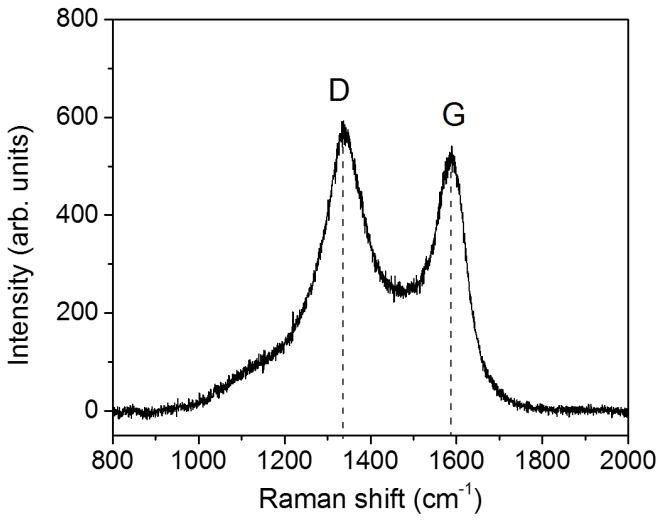

Fig. 4. Raman spectrum (λ = 532 nm) of the pristine carbon black nanoparticles used for dispersion in the PEO electrolyte.

SEM and TEM micrographs reveal that CB nanoparticles are agglomerated in pristine state. Their spherical shape is observed by TEM experiments, and one can note the presence of two main sizes of particles, about 20 and 50 nm in diameter. The Raman spectrum recorded in the 800-2000 cm^{-1} region shows the presence of the typical D and G bands for carbon materials [39].

After the PEO treatment, the processed samples were rinsed with ethanol, cleaned in an ultrasonic bath in ethanol in order to remove all non-incorporated CB nanoparticles, dried, and stored in a dry environment before *ex situ* characterizations.

2.2 *Ex situ* characterization of the PEO coatings

Cross-sections of the processed samples were examined by SEM (FEI – Quanta 650 FEG) working in backscattered electron mode at 20 kV accelerating voltage. Prior to SEM

observations, samples were cut, mounted in resin and finely polished with 1 µm diamond paste. Top surface of the processed samples were observed by SEM in secondary electron mode at 20 kV accelerating voltage. To avoid surface charging issues from improper electron evacuation during SEM observations, the samples were coated with a 10 nm gold thin film. Observations were systematically done at both the centre and the edge of each sample in order to account for possible coating inhomogeneity due to edge effect. The centre and edge areas of the sample are defined as depicted in Fig. 5.

For each zone (edge and centre), the coating thickness was determined as the average value of 40 measurements (20 on each side, front and back, of the sample) taken randomly on the considered zone by an Eddy current gauge (Fischer Isoscope FMP10-FTA3.3H). Moreover, to get a better overview of the variation of thickness over the sample surface, thickness measurements were also done using ImageJ software on SEM cross-section views at rather low magnification. A hundred measurements regularly spaced of 30 µm were taken and averaged in the two zones. The phase composition of the coatings was determined by X-ray diffraction (XRD) measurements in Bragg-Brentano geometry using the Cu-$K_{\alpha 1}$ radiation at λ = 0.1542 nm (Bruker D8 ADVANCE diffractometer). Finally, CB nanoparticles incorporated through the PEO coatings were also characterized by Raman spectroscopy measurements performed with an exciting radiation wavelength of 532 nm in the range 800-2000 cm^{-1}.

Because of the high value of the initial estimates of the sample resistance, electrometric methods must be used to precisely determine the volume conductivity of the composite coatings. Conductivity measurements were performed at room temperature using a Keithley 610BR electrometer in ohmmeter mode. It was connected to the test set-up by a short length coaxial transmission cable and PTFE insulated connectors. The measuring device consisted of

two brass clamps on a PTFE block, shielded by a 2 mm thick copper box. The volume resistance of the coating was measured between a 2.5 cm^2 area covered with silver paint on the surface coating (Fig. 5) and the underlying aluminium substrate.

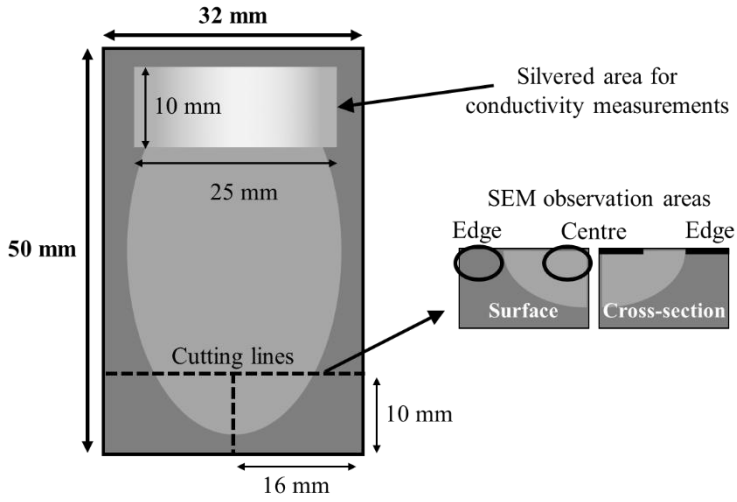

Fig. 5. Schematic drawing showing the SEM observation areas at the centre and at the edge of the PEO processed samples, and the delimited silvered area for conductivity measurements.

3. Results and discussion

3.1 Visual aspects the PEO treated samples.

Fig. 6 shows macroscopic views of the sample surface after PEO treatment for various concentrations of CB nanoparticles dispersed in the electrolyte. Depending on this concentration, the samples exhibit a more or less dark grey colour as compared with the nearly white colour coating of the sample processed without carbon black nanoparticles (CB0). This indicates that carbon nanoparticles are indeed incorporated, at least on the top-most sublayer of the PEO coatings. An inhomogeneity in the colouring can also be observed between the centre and the edges of the samples, the edges being darker in case of a treatment with CB nanoparticles. Such an inhomogeneity is likely due to a stronger electric field at the

edges as already pointed out in references [40, 41], which results in a higher growth rate and likely a greater particle incorporation. Moreover, as the concentration in nanoparticles increases, the visual aspect of the coatings becomes more homogeneous with a larger expansion of the dark zones from the edges to the centre, up to a concentration of 6 $g \cdot L^{-1}$ (CB6).

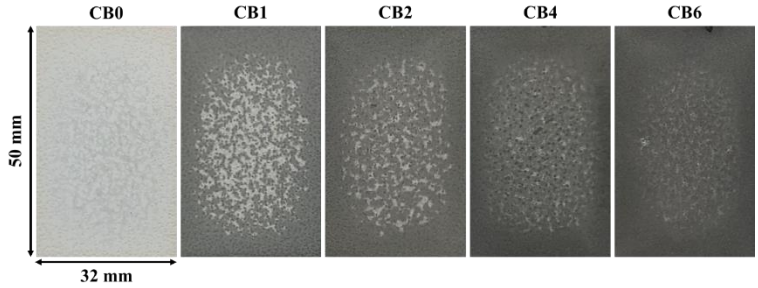

Fig. 6. Macroscopic views of the sample surface after PEO treatment using different concentrations of carbon black nanoparticles dispersed in the electrolyte.

3.2 Morphology of the PEO coatings.

Top–surface SEM micrographs of the processed samples shown in Fig. 7 evidence different morphologies of the PEO layers according to whether they were achieved with or without CB nanoparticles. Sample CB0 exhibits in the centre a mix of a pancake-like morphology as usually reported for PEO processed aluminium samples in silicate-containing electrolyte [2] and a morphology that looks like a pancake-like structure that was damaged, likely because of discharges igniting there. The edge of the sample is only covered with such a damaged pancake-like morphology. Adding CB nanoparticles in the base electrolyte results in a slightly different morphology of the layers that exhibits a sponge-like morphology with few remaining pancake-like structures, with the sponge-like structure covering larger area as the CB concentration in the electrolyte increases. Furthermore, this sponge-like morphology is a well-known feature associated with the "soft" sparking regime as encountered when supplying the

electrodes with a pulse bipolar current waveform having an anodic to cathodic charge quantity ratio slightly lower than 1 [35, 42]. Therefore, this change in surface morphology is likely related to an earlier transition to the "soft" sparking regime when the concentration in carbonaceous nanoparticles in the electrolyte increases. Indeed, we recently reported that the time needed for the PEO process to switch from arc to "soft" sparking regime linearly decreases with the increase in the content of carbon nanoparticles, whether they are carbon nanotubes [43] or carbon black nanoparticles [44]. It is also worth noting that, specifically for the sample CB6 treated in presence of the highest concentration in CB nanoparticles, the surface morphology of the oxide coating is less subject to the edge effect and remains quite similar both at the centre and the edges of the sample (Fig. 7A & 7B), which confirms visual observations (see section 3.1).

At higher magnification (Fig. 7D), SEM observation reveals the presence of nanoparticles in the porosity of the coatings for all samples processed with CB nanoparticles dispersed in the electrolyte. Analyses of the surface of all samples by Raman spectroscopy confirm that these nanoparticles imbedded in the coating surface porosity consist indeed of carbon black nanoparticles (see section 3.5).

The changes in coating morphology are also noticeable on SEM cross-section views (Fig. 8). Sample CB0 exhibits a rather dense inner sublayer and a thin outer sublayer mainly composed of pancake-like structures. In contrast, the sample processed with a low concentration of nanoparticles (CB1) presents a combined arrangement of pancake-like structures and sponge-like ones, while with a higher CB concentration in the electrolyte (CB6), the sponge-like structure dominates and covers the whole sample surface.

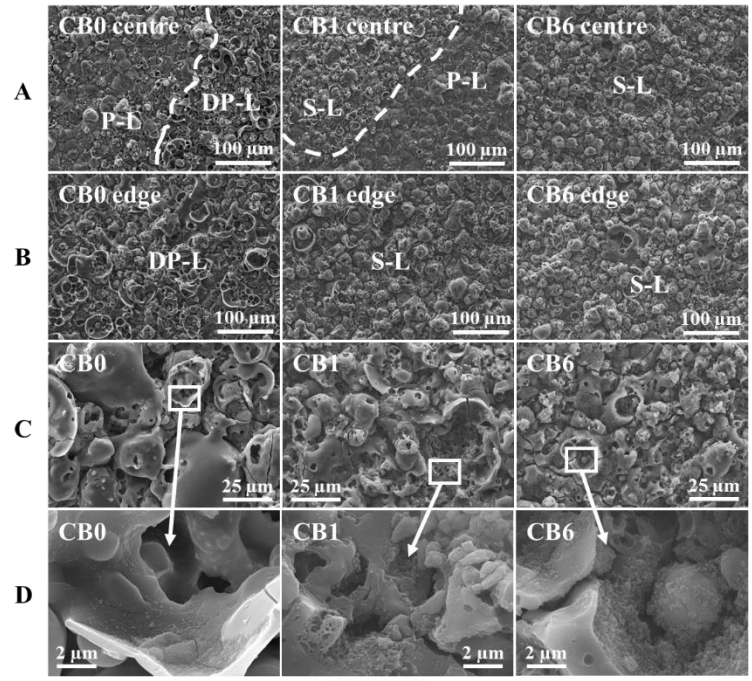

Fig. 7. Top view SEM micrographs of the samples processed with different carbon black concentrations. Low magnification SEM images taken at the centre (A) and at the edge (B) of the samples. Medium (C) and high (D) magnification SEM images showing nanoparticles in the porosity of samples processed with carbon black nanoparticles dispersed in the electrolyte. The dash lines in A delimit zones with different morphology. S-L, P-L, and DP-L stand for sponge-like, pancake-like, and damaged pancake-like structures, respectively.

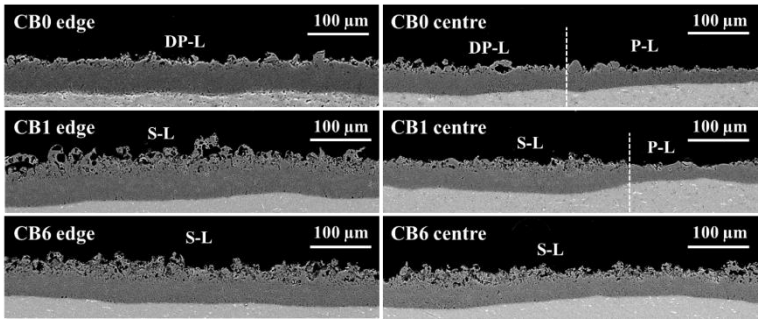

Fig. 8. Cross-section SEM micrographs of the samples processed with different carbon black concentrations. S-L, P-L, and DP-L stand for sponge-like, pancake-like, and damaged pancake-like structures, respectively

3.3 Growth rate of the PEO layers.

As observed on SEM cross-section views (Fig. 8), the effect of introducing CB nanoparticles in the electrolyte on the coating thickness is not that obvious. Therefore, thickness measurements were performed according to the measurement procedures described in section 2.2. Thickness values obtained by using an Eddy current probe (Fig. 9A) show that the average thickness is rather the same whatever the CB concentration dispersed in the electrolyte. However, Eddy current probe has a measurement area of the order of a few square millimetres. To get more localized measurements, thickness values were also determined from cross-section SEM pictures (Fig. 9B). Several observations arise from these measurements. First, the coating inhomogeneity observed on macroscopic views (Fig. 6) is linked to an uneven thickness of the coating over the sample, with a much thicker layer at the edges than at the centre. Second, it appears that the inhomogeneity is less pronounced as the CB concentration in the electrolyte increases, as evidenced by a lower dispersion in the data points (Fig. 9 and Table 4). Third, it is noticeable that the dispersion of thickness values decreases as the concentration in CB increases. Finally, it is worth noting that the sample processed without CB (CB0) exhibits a slightly lower average growth rate than those treated with CB, irrespective of the CB concentration in the electrolyte.

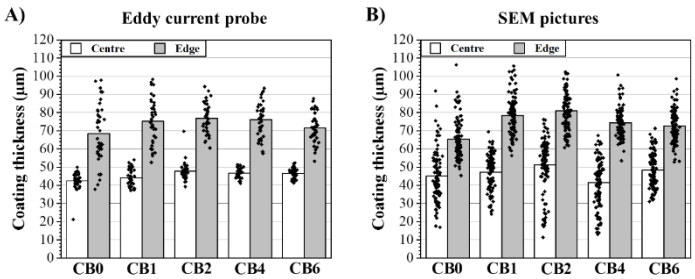

Fig. 9. Coating thickness measured (A) with Eddy current probe and (B) from SEM pictures. Average thickness values in the centre (white bars) and at the edges (grey bars) of the sample,

together with all data points (black dots) that were used to determine the average thickness values. See section 2.2 for the measurement procedure.

Table 4

Standard deviation of coating thickness values measured with Eddy current probe and from SEM pictures.

Sample			CB0	CB1	CB2	CB4	CB6
Standard deviation (µm)	Eddy current	Centre	4.4	4.7	4.7	2.6	2.7
		Edge	15.7	12.1	8.3	9.3	8.0
	SEM	Centre	14.0	9.7	14.8	13.2	9.6
		Edge	10.7	10.8	10.5	8.0	8.6

3.4 Crystallographic phase composition of the PEO coatings

X-ray diffraction (XRD) measurements were carried out in order to identify the different polymorphs of aluminium oxide formed during PEO of aluminium in presence or not of dispersed CB nanoparticles, and to estimate their relative phase proportion. The corresponding X-ray diffraction patterns are shown in Fig. 10. Whatever the concentration in CB, diffraction peaks are fine and well defined, indicating a good crystallinity of the coatings. The aluminium peaks are due to the metallic substrate. All other peaks are due to the PEO coatings in which two main crystalline polymorphic phases of aluminium oxide are detected: the rhombohedral α-Al_2O_3 that corresponds to the stable alumina phase formed at high temperatures (> 1100 °C) and the cubic γ-Al_2O_3 that corresponds to a low temperature metastable phase. Some small diffraction peaks corresponding to monoclinic θ-Al_2O_3 are also detected. As proposed by some authors [45, 46], the relative proportion of α- and γ-Al_2O_3 was

evaluated as a function of the concentration in CB particle from the relative area of the (113) reflexion peak of α-Al_2O_3 at 43.6° (I_α) to that of the (400) one of γ-Al_2O_3 at 45.9° (I_γ). The value of this I_α/I_γ ratio, given in Table 5, is close to 0.5 for all samples suggesting that the presence of CB nanoparticles does not modify the crystallographic phase proportion of PEO oxide coatings achieved on aluminium.

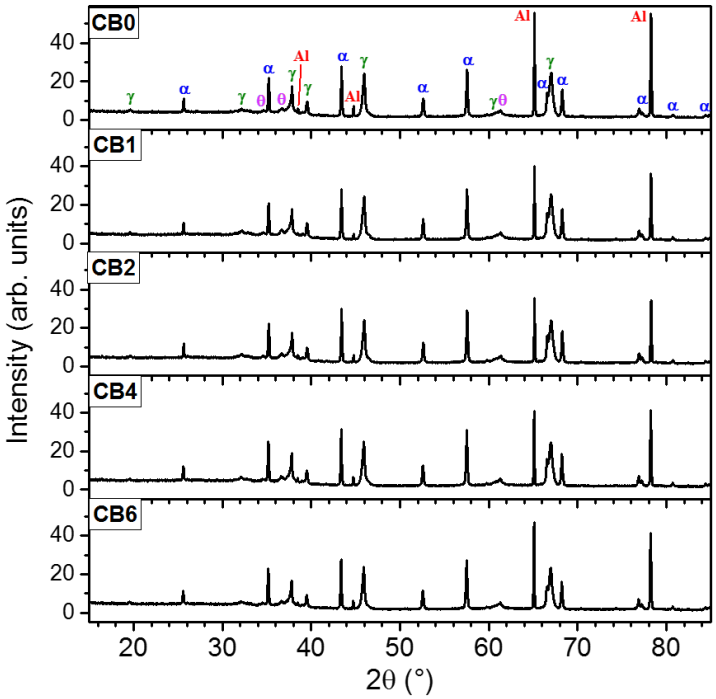

Fig. 10. XRD patterns (Cu-$K_{\alpha1}$, λ = 0.1542 nm) recorded on aluminium samples PEO processed with different concentrations in carbon black nanoparticles dispersed in the electrolyte. **Al** is for aluminium (PDF 04-0787); **α** for α-Al_2O_3 (PDF 46-1212); **γ** for γ-Al_2O_3 (PDF 74-2206) and **θ** for θ-Al_2O_3 (PDF 23-1009).

Table 5

Relative integrated intensity of α-Al_2O_3 (113) and γ-Al_2O_3 (400) diffraction peaks at 43.6° and 45.9°, respectively, for different concentrations of CB nanoparticles.

Sample	CB0	CB1	CB2	CB4	CB6
I_α/I_γ	0.49	0.43	0.48	0.49	0.51

3.5 Characterization of PEO coatings by Raman spectroscopy

Fig. 11 shows the Raman spectra recorded on the surface (at the edge area) of CB0, CB1, and CB6 samples. As a reminder, data from Fig. 4 (multiplied by 4 for an easier comparison) are also plotted in Fig. 11. As expected, no vibrational band of CB is detected for sample CB0 processed without nanoparticles. In contrast, for samples CB1 and CB6, the spectra reveal two bands attributed to carbon nanoparticles: the D band around 1350 cm^{-1} associated with the structural defects of the carbon black nanoparticles, and the G band around 1600 cm^{-1} due to the in-plane vibrations of sp^2 carbon atoms. It is also worth noting that the spectra of the CB1 and CB6 samples are superimposable, which means that increasing the concentration of CB in the electrolyte does not modify the structural properties of the incorporated CB nanoparticles. Moreover, the comparison of these spectra with that of the pristine CB nanoparticles does not evidence any significant difference, thus indicating that incorporated CB nanoparticles are not degraded by the PEO process. These results clearly show that CB nanoparticles are efficiently incorporated in the PEO coating, without being damaged.

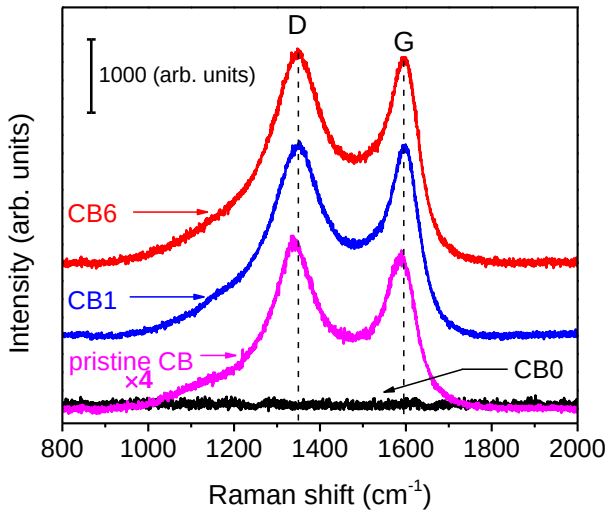

Fig. 11. Raman spectra (λ = 532 nm) of the surface of PEO coatings obtained with different concentrations in carbon black nanoparticles dispersed into the electrolyte (0, 1 and 6 g·L^{-1}). Spectra were recorded at the edge area of the samples.

3.6 Electrical properties of the PEO coatings

The volume conductivity σ_V (S·cm^{-1}) was calculated from the volume resistance value R_V (Ω) according to the following equation:

$$\sigma_V = \frac{1}{R_V} \times \frac{e}{A} \quad (1)$$

where e (cm) is the average thickness of the coating measured on the edge of the sample by Eddy current probe, and A (cm^2) is the area of the measuring zone.

The values given in Table 6 show a volume conductivity of the order of 10^{-12} S·cm^{-1}, which corresponds to values reported for usual porous alumina layers like those deposited by thermal spray [47-49], with some defects and/or impurities.

Values vary slightly, but remain within this range, despite the incorporation of carbon black nanoparticles in the layers.

Table 6

Volume resistance R_V and volume electrical conductivity σ_V of the PEO coatings obtained with different CB concentrations dispersed into the electrolyte.

Sample	CB0	CB1	CB2	CB4	CB6
R_V (10^9 Ω)	1.65	1.45	1.50	1.05	2.25
σ_V (10^{-12} S·cm^{-1})	1.65	2.07	2.05	2.90	1.28

3.7 Discussion

From the results and observations presented above, it can be suggested that the CB nanoparticles do not incorporate deeply in the layers and are likely located in the outer porous sublayer. To sustain this hypothesis, Raman spectra were recorded along the coating thickness of sample CB6. For this, the coating was detached from the aluminium substrate by immersing the sample in a 1M NaOH solution for about 2 hours. After dissolution of the substrate, the resulting self-supported layer was broken to reveal the transverse coating cross section on which Raman spectroscopy was performed. This cross section was also observed using a ZEISS Gemini SEM 500 in SE mode at 2 kV accelerating voltage, which allowed us to work without depositing a conductive gold layer prior to the observations. Fig. 12 shows the Raman spectra recorded at various depths of the coating, together with a SEM micrograph on which the locations of the measurement points are reported.

These spectra clearly evidence that carbon particles are only detected in the outer porous sublayer. This is in agreement with the incorporation mechanism driven by the electrolyte filling the pores left after the extinction of micro-discharges ignited at the surface, as proposed by O'Hara *et al.* [13] and by Da Silva Tousch *et al.* [50]. Nevertheless, the absence of CB fingerprint in the dense sublayer does not necessarily mean that no particles are trapped in that sublayer. It could be also that CB nanoparticles be embedded in that sublayer with an amount

below the Raman detection limit, which would also be consistent with the results of electrical conductivity measurements.

The preferential incorporation in the outer sublayer is also consistent with the macroscopic views of the samples (Fig. 6) and the related SEM observations (Fig. 7 & 8). Indeed, as the CB concentration in the electrolyte increases, the sponge-like structure expands on larger area on the sample. Such a structure has a higher porosity and, consequently, more sites in which CB particles can be trapped. This results in a more homogeneous black colour of the samples processed with a high CB concentration (Fig. 6).

As for the electrical conduction properties of the carbon-alumina composite, two issues must be addressed. First, the CB nanoparticles must be evenly distributed across the layer thickness. One possibility could be to favour the porous layer and inhibit the growth of the dense inner layer by working out of soft sparking conditions [35, 36]. It is also well known that supplying the electrodes with DC current or voltage favours the growth of porous PEO coatings on aluminium [51]. Such a DC mode could therefore be of interest to incorporate more particles into the layers. Incorporating CB nanoparticles into the dense sublayer could also be a solution to grow a carbon-alumina conductive composite, similarly to carbon-polymer conductive composites [32, 33]. This however is still a concern since the dense layer can be formed either by diffusion mechanisms of aluminium and oxygen species from the substrate and the electrolyte respectively, or by densification of the porous layer under soft sparking conditions. In the former case, CB nanoparticles could unlikely penetrate the dense layer. In the latter case, one would expect CB nanoparticles present in the porous layer to be trapped in the densified layer, which would be an asset towards conductive PEO layers. Second, incorporated CB nanoparticles must percolate in order to constitute a continuous current pathway. This implies that most of the inner pores are open in order to form a network of cavities that could be filled with CB nanoparticles.

Increasing the porosity would however likely be detrimental to the corrosion and wear resistance of the coatings, which might be an issue depending on the applications.

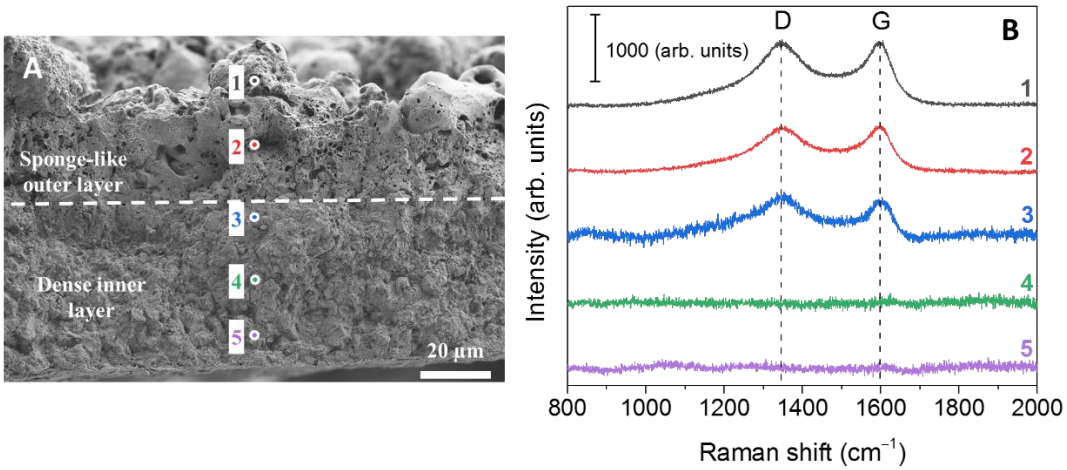

Fig. 12. A) SEM micrograph of a cross section of a self-supported PEO layer (CB6) with indication of the points where Raman spectra were recorded. B) Raman spectra (λ = 532 nm) recorded at several depths across the layer as indicated in the SEM image in A).

4. Conclusions

The present study related to the incorporation of carbon black nanoparticles (CB) into alumina layers formed by plasma electrolytic oxidation of aluminium with carbon black nanoparticles dispersed at various concentrations in the processing electrolyte. In particular, the main objective was to take advantage of complementary characterization techniques to study how the presence of CB influences the produced PEO alumina coating and its characteristics including the electrical volume conductivity. The information presented allows the following conclusions to be drawn:

- CB preferentially incorporate throughout the sponge-like structure of the coating. Moreover, the increase in the CB concentration promotes a larger covering of the sponge-like structure, and a higher incorporation of CB nanoparticles into the overall processed surface.

- The presence of CB nanoparticles results in a slight increase in the average growth rate of the PEO coatings (as compared with processing without particles). Whatever the concentration in CB nanoparticles, the average growth rate of the PEO coatings remains close to 1.2 $\mu m \cdot min^{-1}$.
- CB do not affect the crystallographic phase composition and coatings mainly consist of α and γ-alumina polymorphs in more or less identical proportion.
- CB nanoparticles do not seem to undergo any structural degradation from the surrounding plasma of the micro-discharges.
- In the range of 0 to 6 $g \cdot L^{-1}$ CB concentration in the electrolyte, the electrical volume conductivity remains constant at about 10^{-12} $S \cdot cm^{-1}$. It is therefore suspected that because incorporation mainly takes place in the outermost porous sublayer, the percolation threshold through the dense inner sublayer is not being reached.

Acknowledgments

- This work was funded by the French Agence Nationale de la Recherche (ANR) under project CAMFRE - ANR21-CE08-0029
- The authors acknowledge the Conseil Régional de la Région Grand Est for granting C. Da Silva Tousch's PhD work under decision 19_GE_049.
- The contribution of the characterization platforms of Institut Jean Lamour is highly acknowledged.
- The authors greatly acknowledge Mrs Anna Nomine for her contribution in TEM characterization of carbon black nanoparticles, and the MPA team at Institut Jean Lamour for the realization of some parts or the experimental device by additive manufacturing.

Data availability

The data that support the findings of this study are available from the corresponding author, upon reasonable request.

Declaration of competing interest

The authors declare no competing financial interests.

CRediT author statement

L. Magniez: Methodology, investigation, formal analysis, methodology, visualization, writing - original draft, writing - review & editing.

C. Da Silva Tousch: Methodology, investigation, formal analysis, writing - review & editing.

S. Fontana: Formal analysis, supervision, writing - review & editing.

S. Cahen: Formal analysis, supervision, writing - review & editing.

J. Martin: Conceptualisation, formal analysis, supervision, methodology, writing - review & editing.

C. Hérold: Supervision, formal analysis, writing – review & editing.

G. Henrion: Conceptualization, supervision, project administration, funding acquisition, writing – review & editing.

Authorship statement

The submission of the manuscript has been approved by all co-authors.

References

1. A.L. Yerokhin, X. Nie, A. Leyland, A. Matthews, S.J. Dowey, Plasma electrolysis for surface engineering, Surf. Coat. technol. 122 (1999) 73-93. https://doi.org/10.1016/S0257-8972(99)00441-7

2. G. Sundararajan, L. Rama Krishna, Mechanisms underlying the formation of thick alumina coatings through the MAO coating technology, Surf. Coat. technol. 167 (2003) 269-277. https://doi.org/10.1016/S0257-8972(02)00918-0

3. D. Veys-Renaux, E. Rocca, G. Henrion, Micro-arc oxidation of AZ91 Mg alloy: An in-situ electrochemical study, Electrochem. Commun. 31 (2013) 42-45. http://dx.doi.org/10.1016/j.elecom.2013.02.023

4. M. Toorani, M. Aliofkhazraei, Review of electrochemical properties of hybrid coating systems on Mg with plasma electrolytic oxidation process as pretreatment, Surf. Interfaces 14 (2019) 262–295. https://doi.org/10.1016/j.surfin.2019.01.004

5. M. Aliofkhazraei, D.D. Macdonald, E. Matykina, E.V. Parfenov, V.S. Egorkin, J.A. Curran, S.C. Troughton, S.L. Sinebryukhov, S.V. Gnedenkov, T. Lampke, F. Simchen, H.F. Nabavi, Review of plasma electrolytic oxidation of titanium substrates: Mechanism, properties, applications and limitations, Appl. Surf. Sci. Adv. 5 (2021) 100121. https://doi.org/10.1016/j.apsadv.2021.100121

6. S. Sikdar, P.V. Menezes, R. Maccione, T. Jacob, P.L. Menezes, Plasma electrolytic oxidation (PEO) process—processing, properties, and applications, Nanomat. 11 (2021) 1375. https://doi.org/10.3390/nano11061375

7. X. Lu, C. Blawert, Y. Huang, H. Ovri, M.L. Zheludkevich, K.U. Kainer, Plasma electrolytic oxidation coatings on Mg alloy with addition of SiO_2 particles, Electrochim. Acta 187 (2016) 20-33. https://dx.doi.org/10.1016/j.electacta.2015.11.033

8. X.P. Lu, M. Mohedano, C. Blawert, E. Matykina, R. Arrabal, K.U. Kainer, M.L. Zheludkevich, Plasma electrolytic oxidation coatings with particle additions - A review, Surf. Coat. Technol. 307 (2016) 1165-1182. https://dx.doi.org/10.1016/j.surfcoat.2016.08.055

9. B.S. Necula, L.E. Fratila-Apachitei, S.A.J. Zaat, I. Apachitei, J. Duszczyk, In vitro antibacterial activity of porous TiO_2–Ag composite layers against methicillin-resistant

Staphylococcus aureus, Acta Biomater. 5 (2009) 3573-3580.
https://dx.doi.org/10.1016/j.actbio.2009.05.010

10 H. Nasiri Vatan, R. Ebrahimi-kahrizsangi, M. Kasiri-asgarani, Structural, tribological and electrochemical behavior of SiC nanocomposite oxide coatings fabricated by plasma electrolytic oxidation (PEO) on AZ31 magnesium alloy, J. Alloys Compd. 683 (2016) 241-255.
https://dx.doi.org/10.1016/j.jallcom.2016.05.096

11 D. Kim, D. Sung, J. Lee, Y. Kim, W. Chung, Composite plasma electrolytic oxidation to improve the thermal radiation performance and corrosion resistance on an Al substrate, Appl. Surf. Sci. 357 (2015) 1396-1402.
https://dx.doi.org/10.1016/j.apsusc.2015.10.003

12 M. Shokouhfar, S.R. Allahkaram, Formation mechanism and surface characterization of ceramic composite coatings on pure titanium prepared by micro-arc oxidation in electrolytes containing nanoparticles, Surf. Coat. Technol. 291 (2016) 396-405.
https://dx.doi.org/10.1016/j.surfcoat.2016.03.013

13 M. O'Hara, S.C. Troughton, R. Francis, T.W. Clyne, The incorporation of particles suspended in the electrolyte into plasma electrolytic oxidation coatings on Ti and Al substrates, Surf. Coat. Technol. 385 (2020) 125354.
https://doi.org/10.1016/j.surfcoat.2020.125354

14 M. Kaseem, S. Fatimah, N. Nashrah, Y.G. Ko, Recent progress in surface modification of metals coated by plasma electrolytic oxidation: Principle, structure, and performance, Prog. Mater. Sci. 117 (2021) 100735.
https://doi.org/10.1016/j.pmatsci.2020.100735

15 X.P. Lu, C. Blawert, M.L. Zheludkevich, K.U. Kainer, "Insights into plasma electrolytic oxidation treatment with particle addition", Corr. Sci. 101 (2015) 201-207.
https://dx.doi.org/10.1016/j.corsci.2015.09.016

16 K.M. Lee, B.U. Lee, S.I. Yoon, E.S. Lee, B. Yoo, D.H. Shin, Evaluation of plasma temperature during plasma oxidation processing of AZ91Mg alloy through analysis of the melting behavior of incorporated particles, Electrochim. Acta 67 (2012) 6-11.
https://dx.doi.org/10.1016/j.electacta.2012.01.053

17 W.K. Yeung, I.V. Sukhorukova, D.V. Shtansky, E.A. Levashov, I.Y. Zhitnyak, N.A. Gloushankova, P.V. Kiryukhantsev-Korneev, M.I. Petrzhik, A. Matthews, A. Yerokhin, Characteristics and in vitro response of thin hydroxyapatite-titania films produced by plasma electrolytic oxidation of Ti alloys in electrolytes with particle additions, RSC Adv. 6 (2016) 12688-12698.
https://dx.doi.org/10.1039/c5ra22178a

18 B.S. Necula, L.E. Fratila-Apachitei, A. Berkani, I. Apachitei, J. Duszczyk, Enrichment of anodic MgO layers with Ag nanoparticles for biomedical applications, J. Mater. Sci. Mater. Med. 20 (2009) 339-345. https://dx.doi.org/10.1007/s10856-008-3589-9

19 K.M. Lee, Y.G. Ko, D.H. Shin, Incorporation of multi-walled carbon nanotubes into the oxide layer on a 7075 Al alloy coated by plasma electrolytic oxidation: coating structure and corrosion properties, Curr. Appl. Phys. 11 (2011) S55-S59. https://dx.doi.org/10.1016/j.cap.2011.07.009

20 X. Li, B.L. Luan, Discovery of Al2O3 particles incorporation mechanism in plasma electrolytic oxidation of AM60B magnesium alloy, Mater. Lett. 86 (2012) 88-91. https://dx.doi.org/10.1016/j.matlet.2012.07.032

21 R. Arrabal, M. Mohedano, E. Matykina, A. Pardo, B. Mingo, M.C. Merino, Characterization and wear behaviour of PEO coatings on 6082-T6 aluminium alloy with incorporated α-Al2O3 particles, Surf. Coat. Technol. 269 (2015) 64-73. https://dx.doi.org/10.1016/j.surfcoat.2014.10.048

22 J. Martin, A. Nominé, V. Ntomprougkidis, S. Migot, S. Bruyère, F. Soldera, T. Belmonte, G. Henrion, Formation of a metastable nanostructured mullite during plasma electrolytic oxidation of aluminium in "soft" regime condition, Mater. & Design 180 (2019) 107977. https://dx.doi.org/10.1016/j.matdes.2019.107977

23 M.A. Chen, Y.C. Ou, Y.H. Fu, Z.H. Li, J.M. Li, S.D. Liu, Effect of friction stirred Al-Fe-Si particles in 6061 aluminum alloy on structure and corrosion performance of MAO coating, Surf. Coat. Technol. 304 (2016) 85-97. http://dx.doi.org/10.1016/j.surfcoat.2016.07.003

24 Y. Chen, X.P. Lu, C. Blawert, M.L. Zheludkevich, T. Zhang, F.H. Wang, Formation of self-lubricating PEO coating via in-situ incorporation of PTFE particles, Surf. Coat. Technol. 337 (2018) 379-388. https://doi.org/10.1016/j.surfcoat.2018.01.022

25 X.Y. Li, C.F. Dong, Q. Zhao, Y. Pang, F.S. Cheng, S.X. Wang, Characterization of microstructure and wear resistance of PEO coatings containing various microparticles on Ti6Al4V alloy, J. Mater. Eng. Perf. 27 (2018) 1642-1653. https://doi.org/10.1007/s11665-018-3249-2

26 X. Wu, H.X. Li, J.P. Lu, Y.Y. Li, C.B. Yang, Y.H. Cen, Z.T. Yang, R.G. Song, MoS_2 additive to the MAO Al_2O_3 composite coatings with enhanced mechanical performances, Mater. Res. Express 6 (2019) 016543. https://doi.org/10.1088/2053-1591/aae704

27 From a search performed in June 2023 using the Web of Science platform (https://www.webofscience.com/wos/) with the combined keywords (microarc oxidation OR plasma electrolytic oxidation) AND (particles) AND (carbon OR graphite).

28 A. Kausar, Contemporary applications of carbon black-filled polymer composites: An overview of essential aspects, J. Plast. Film Sheeting 34 (2018) 256-299. https://doi.org/10.1177/8756087917725773

29 J.C. Biermann, M.J. Wetterwald, J. Messiet, J. Lahaye, Chemical behavior of conductive carbon-blacks in Leclanche type batteries, Electrochim. Acta 26 (1981) 1237-1239. https://doi.org/10.1016/0013-4686(81)85104-3

30 R. Alcantara, J.M. Jimenez-Mateos, P. Lavela, P, J.L. Tirado, Carbon black: a promising electrode material for sodium-ion batteries, Electrochem. Commun. 3 (2001) 639-642. https://doi.org/10.1016/S1388-2481(01)00244-2

31 J. Hu, S. Zhong, T. Yan, Using carbon black to facilitate fast charging in lithium-ion batteries, J. Power Sources 208 (2021) 230342. https://doi.org/10.1016/j.jpowsour.2021.230342

32 J.C. Huang, Carbon black filled conducting polymers and polymer blends, Adv. Polym. Technol. 21 (2002) 299-313. https://doi.org/10.1002/adv.10025

33 F. Orozco, A. Salvatoreb, A. Sakulmankongsuk, D.R. Gomes, Y. Pei, E. Araya-Hermosilla, A. Pucci, I. Moreno-Villoslada, F. Picchioni, R.K. Bose, Electroactive performance and cost evaluation of carbon nanotubes and carbon black as conductive fillers in self-healing shape memory polymers and other composites, Polymer 260 (2022) 125365. https://doi.org/10.1016/j.polymer.2022.125365

34 J. Beauvir, Oxidising electrolytic method for obtaining a ceramic coating at the surface of a metal, Patent WO 01/81658 A1 (2001).

35 F. Jaspard-Mécuson, T. Czerwiec, G. Henrion, T. Belmonte, L. Dujardin, A. Viola, J. Beauvir, Tailored aluminium oxide layers by bipolar current adjustment in the plasma electrolytic oxidation (PEO) process, Surf. Coat. Technol. 201 (2007) 8677-8682. https://doi.org/10.1016/j.surfcoat.2006.09.005

36 D.-S. Tsai, C.-C. Chou, Review of the soft sparking issues in plasma electrolytic oxidation, Metal 8 (2018) 1015. https://doi.org/10.3390/met8020105

37 A.B. Rogov, A. Nemcova, T. Hashimoto, A. Matthews, A. Yerokhin, Analysis of electrical response, gas evolution and coating morphology during transition to soft

sparking PEO of Al, Surf. Coat. Technol. 442 (2022) 128142. https://doi.org/10.1016/j.surfcoat.2022.128142

38 J. Martin, P. Leone, A. Nominé, D. Veys-Renaux, G. Henrion, T. Belmonte, Influence of electrolyte ageing on the plasma electrolytic oxidation of aluminium, Surf. Coat. Techno. 269 (2015) 36-46 http://dx.doi.org/10.1016/j.surfcoat.2014.11.001

39 A. Merlen, J. Buijnsters, C. Pardanaud, A guide to and review of the use of multiwavelength Raman spectroscopy for characterizing defective aromatic carbon solids: from graphene to amorphous carbons, Coatings 7 (2017) 153. https://doi.org/10.3390/coatings7100153

40 E. Matykina, R. Arrabal, P. Skeldon, G.E. Thompson, P. Belenguer, AC PEO of aluminium with porous alumina precursor films, Surf. Coat. Technol. 205 (2010) 1668–1678. https://doi.org/10.1016/j.surfcoat.2010.05.014

41 J. Martin, A. Melhem, I. Shchedrina, T. Duchanoy, A. Nominé, G. Henrion, T. Czerwiec, T. Belmonte, Effects of electrical parameters on plasma electrolytic oxidation of aluminium, Surf. Coat. Technol. 221 (2013) 70-76 https://doi.org/10.1016/j.surfcoat.2013.01.029

42 V. Ntomprougkidis, J. Martin, A. Nominé, G. Henrion, Sequential run of the PEO process with various pulsed bipolar current waveforms, Surf. Coat. Technol. 374 (2019) 713-724. https://doi.org/10.1016/j.surfcoat.2019.06.057

43 C. Da Silva Tousch, L. Magniez, S. Fontana, G. Marcos, C. Hérold, G. Henrion, T. Czerwiec, J. Martin, Influence of carbon nanotubes on the plasma electrolytic oxidation process of aluminum under “soft” sparking conditions, Surf. Coat. Technol. 468 (2023) 129779. https://doi.org/10.1016/j.surfcoat.2023.129779

44 L. Magniez, C. Da Silva Tousch, S. Fontana, J. Martin, T. Czerwiec, C. Hérold, G. Henrion, How carbon black nanoparticles affect the occurrence of soft-sparking during plasma electrolytic oxidation, Materials Letters 350 (2023) 134960. https://doi.org/10.1016/j.matlet.2023.134960

45 W. Xue, Z. Deng, Y. Lai, R. Chen, Analysis of phase distribution for ceramic coatings formed by microarc oxidation on aluminium alloy, J. Am. Ceram. Soc. 81 (1998) 1365-1368. https://dx.doi.org/10.1111/j.1151-2916.1998.tb02493.x

46 A L Yerokhin, L O Snizhko, N L Gurevina, A Leyland, A Pilkington, A Matthews, Discharge characterization in plasma electrolytic oxidation of aluminium, J. Phys. D:

Appl. Phys. 36 (2003) 2110–2120.
http://dx.doi.org/10.1088/0022-3727/36/17/314

47 Y.S. Pirogov, R.M. Brown, A.L. Friedberg, Electrical properties of Al_2O_3-nickel metal multilayer flame sprayed coatings, Am. Ceram. Soc. Bull. 45 (1966) 1071-1074.

48 L. Pawłoski, The relationship between structure and dielectric properties in plasma-sprayed alumina coatings, Sur. Coat. Technol. 35 (1988) 285-298
https://doi.org/10.1016/0257-8972(88)90042-4

49 M. Hauer, M. Meyer, D. Billieres, C. Bricquet, F. Gerstgrasser, J. Kiilakoski, J. Lejay, K.-M. Henkel, Use of different process gases for manufacturing isolating alumina coatings by flame spraying with cords, J. Therm. Spray Tech. 30 (2021) 222-235
https://doi.org/10.1007/s11666-021-01160-8

50 C. Da Silva Tousch, J. Martin, G. Marcos, T. Czerwiec, G. Henrion, Evidence of in-depth incorporation of carbon nanotubes in alumina layers grown by plasma electrolytic oxidation, Surf. Coat. Technol. 440 (2022) 128489
https://doi.org/10.1016/j.surfcoat.2022.128489

51 S. Xin, L. Song, R. Zhao, X. Hu, Influence of cathodic current on composition, structure and properties of Al_2O_3 coatings on aluminum alloy prepared by micro-arc oxidation process, Thin Solid Films 515 (2006), 326–332.
http://dx.doi.org/10.1016/j.tsf.2005.12.087

List of Tables

Table 1

Elemental composition of the 1050 aluminium substrate.

Element	Fe, Ti, Zn	Si	Cu	Mg	Mn	Al
wt.%	< 0.5	< 0.25	0.05	< 0.05	< 0.05	Balance

Table 2

Parameters of the current waveform.

Current pulse frequency (Hz)		100
Anodic current pulse	Rise time (ms)	0.6
	Pulse duration (ms)	2.6
	Fall time (ms)	0.3
	Amplitude (A)	15
	Charge per pulse (C)	0.046
Delay between anodic and cathodic pulses (ms)		0.3
Cathodic current pulse	Rise time (ms)	0.3
	Pulse duration (ms)	5.5
	Fall time (ms)	0.3
	Amplitude (A)	-9
	Charge per pulse (C)	0.052
Delay between cathodic and anodic pulses (ms)		0.1

Table 3

Concentration of dispersed carbon black nanoparticles used in different electrolytes, and corresponding sample identification.

CB ($g \cdot L^{-1}$)	0	1	2	4	6
Sample name	CB0	CB1	CB2	CB4	CB6

Table 4

Standard deviation of coating thickness values measured with Eddy current probe and from SEM pictures.

Sample			CB0	CB1	CB2	CB4	CB6
Standard deviation (µm)	Eddy current	Centre	4.4	4.7	4.7	2.6	2.7
		Edge	15.7	12.1	8.3	9.3	8.0
	SEM	Centre	14.0	9.7	14.8	13.2	9.6
		Edge	10.7	10.8	10.5	8.0	8.6

Table 5

Relative integrated intensity of α-Al_2O_3 (113) and γ-Al_2O_3 (400) diffraction peaks at 43.6° and 45.9°, respectively, for different concentrations of CB nanoparticles.

Sample	CB0	CB1	CB2	CB4	CB6
I_α/I_γ	0.49	0.43	0.48	0.49	0.51

Table 6

Volume resistance R_V and volume electrical conductivity σ_V of the PEO coatings obtained with different CB concentrations dispersed into the electrolyte.

Sample	CB0	CB1	CB2	CB4	CB6
R_V (10^9 Ω)	1.65	1.45	1.50	1.05	2.25
σ_V (10^{-12} S·cm^{-1})	1.65	2.07	2.05	2.90	1.28

Figure captions.

Fig. 1. Experimental setup for PEO treatments with dispersed carbon black nanoparticles in the electrolyte.

Fig. 2. Schematic drawing of one period of the current waveform indicating the time at each change in the current rising/falling rate according to Table 2.

Fig. 3. TEM (A) and SEM (B) micrographs of the pristine carbon black nanoparticles used for dispersion in the PEO electrolyte.

Fig. 4. Raman spectrum (λ = 532 nm) of the pristine carbon black nanoparticles used for dispersion in the PEO electrolyte.

Fig. 5. Schematic drawing showing the SEM observation areas at the centre and at the edge of the PEO processed samples, and the delimited silvered area for conductivity measurements.

Fig. 6. Macroscopic views of the sample surface after PEO treatment using different concentrations of carbon black nanoparticles dispersed in the electrolyte.

Fig. 7. Top view SEM micrographs of the samples processed with different carbon black concentrations. Low magnification SEM images taken at the centre (A) and at the edge (B) of the samples. Medium (C) and high (D) magnification SEM images showing nanoparticles in

the porosity of samples processed with CB nanoparticles dispersed in the electrolyte. The dash lines in A delimit zones with different morphology. S-L, P-L, and DP-L stand for sponge-like, pancake-like, and damaged pancake-like structures, respectively.

Fig. 8. Cross-section SEM micrographs of the samples processed with different carbon black concentrations. S-L, P-L, and DP-L stand for sponge-like, pancake-like, and damaged pancake-like structures, respectively

Fig. 9. Coating thickness measured (A) with Eddy current probe and (B) from SEM pictures. Average thickness values in the centre (white bars) and at the edges (grey bars) of the sample, together with all data points (black dots) that were used to determine the average thickness values. See section 2.2 for the measurement procedure.

Fig. 10. XRD patterns (Cu-$K_{\alpha 1}$, λ = 0.1542 nm) recorded on aluminium samples PEO processed with different concentrations in carbon black nanoparticles dispersed in the electrolyte. **Al** is for aluminium (PDF 04-0787); **α** for α-Al_2O_3 (PDF 46-1212); **γ** for γ-Al_2O_3 (PDF 74-2206) and **θ** for θ-Al_2O_3 (PDF 23-1009).

Fig. 11. Raman spectra (λ = 532 nm) of the surface of PEO coatings obtained with different concentrations in carbon black nanoparticles dispersed into the electrolyte (0, 1 and 6 $g \cdot L^{-1}$). Spectra were recorded at the edge area of the samples.

Fig. 12. A) SEM micrograph of a cross section of a self-supported PEO layer (CB6) with indication of the points where Raman spectra were recorded. B) Raman spectra (λ = 532 nm) recorded at several depths across the layer as indicated in the SEM image in A).

List of Figures

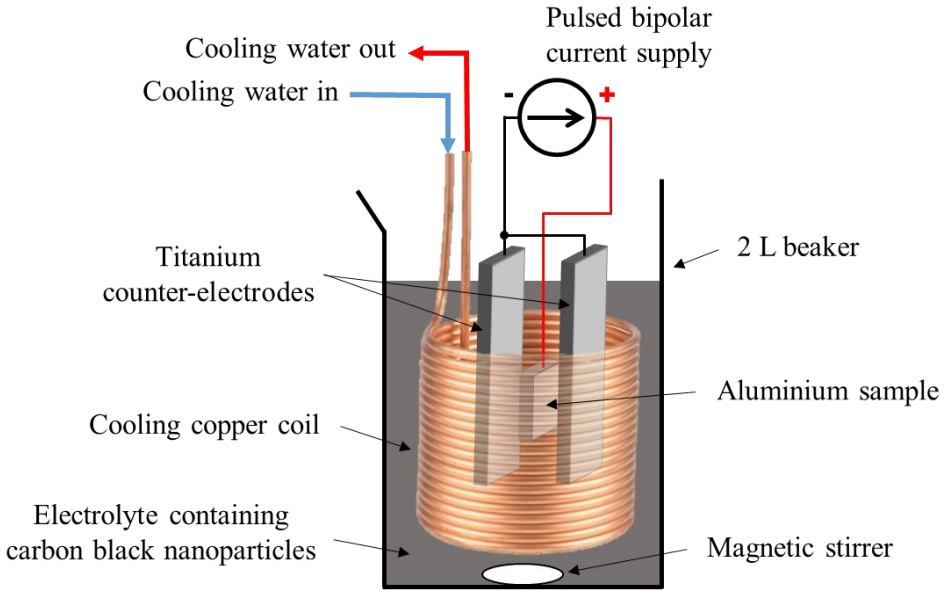

Fig. 1.

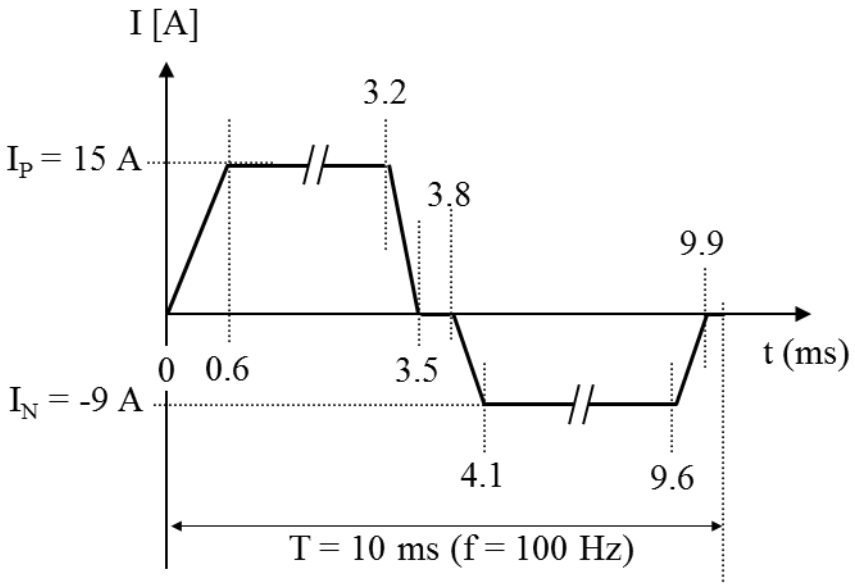

Fig. 2.

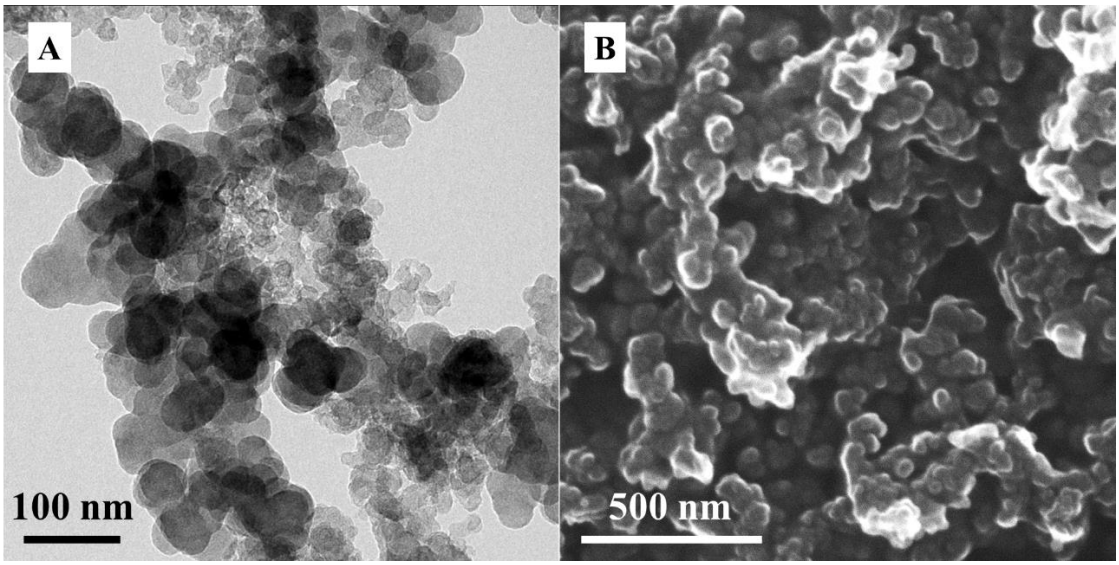

Fig. 3.

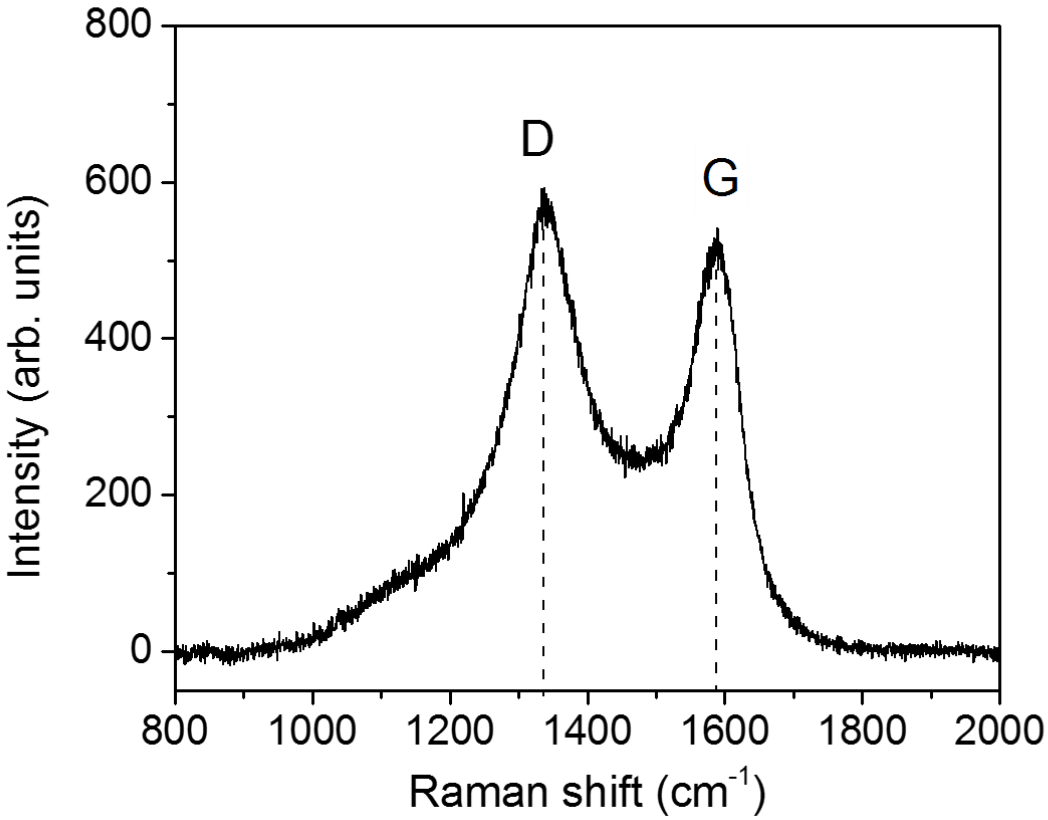

Fig. 4.

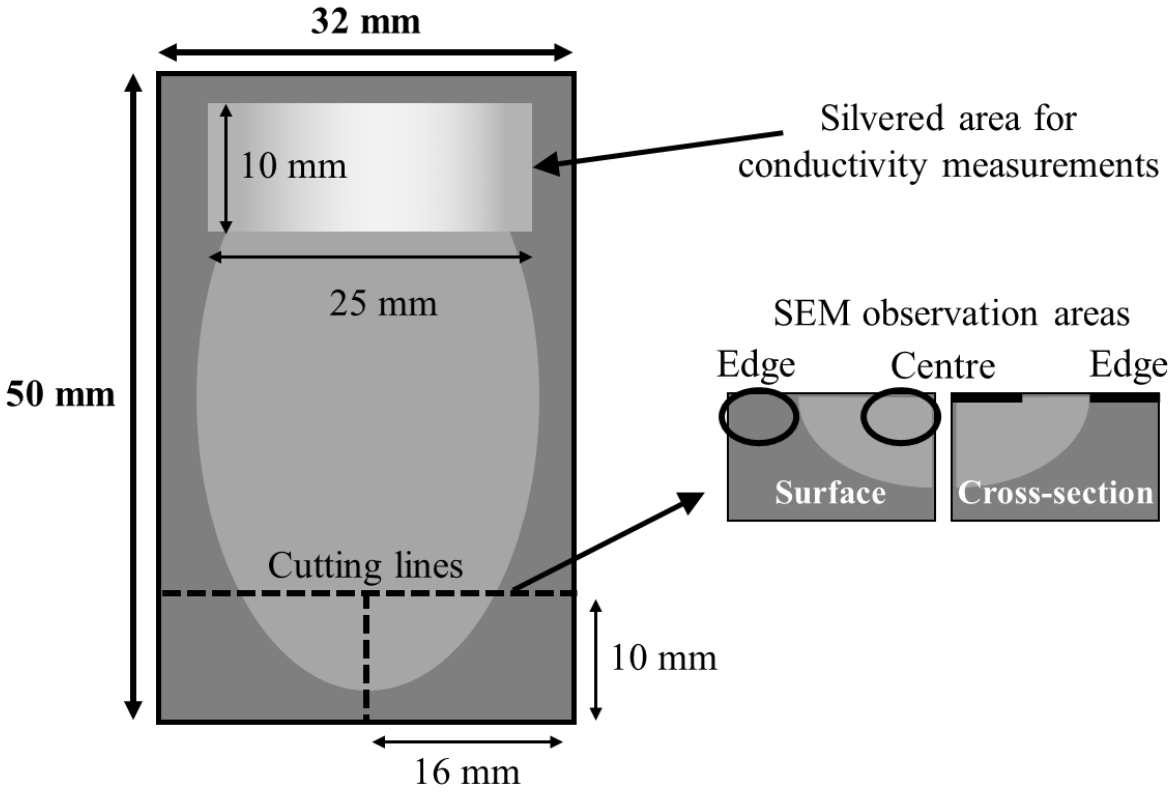

Fig. 5.

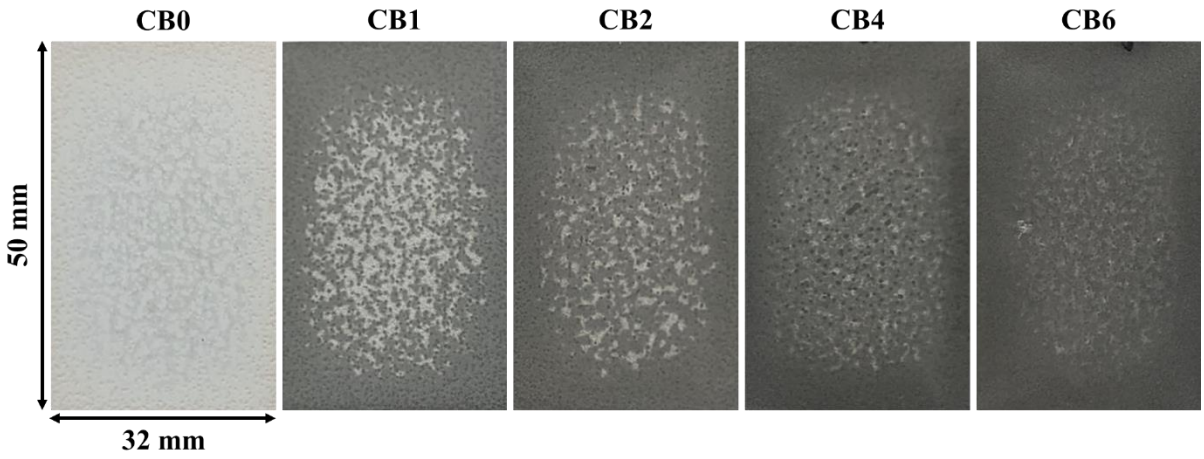

Fig. 6.

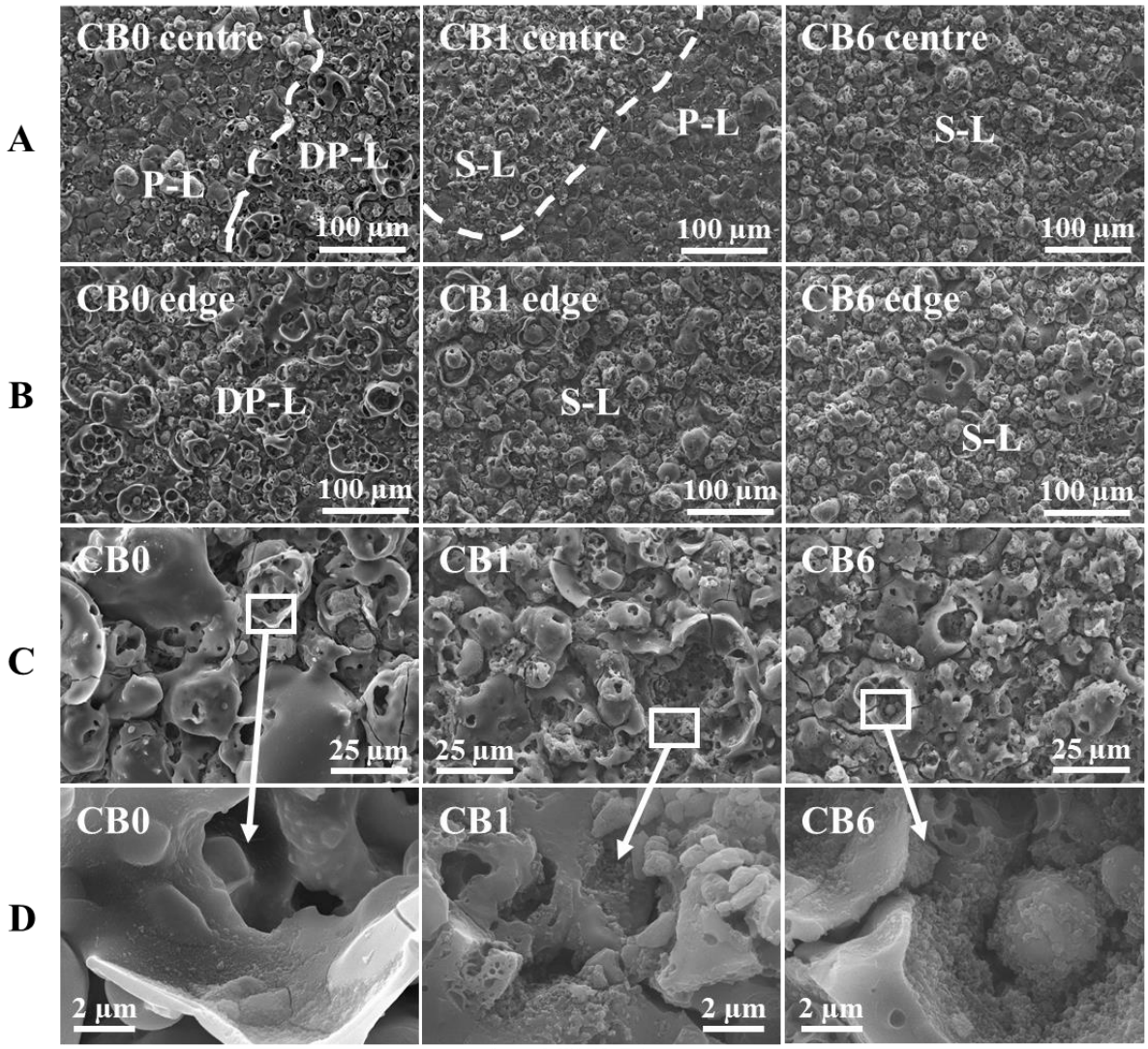

Fig. 7.

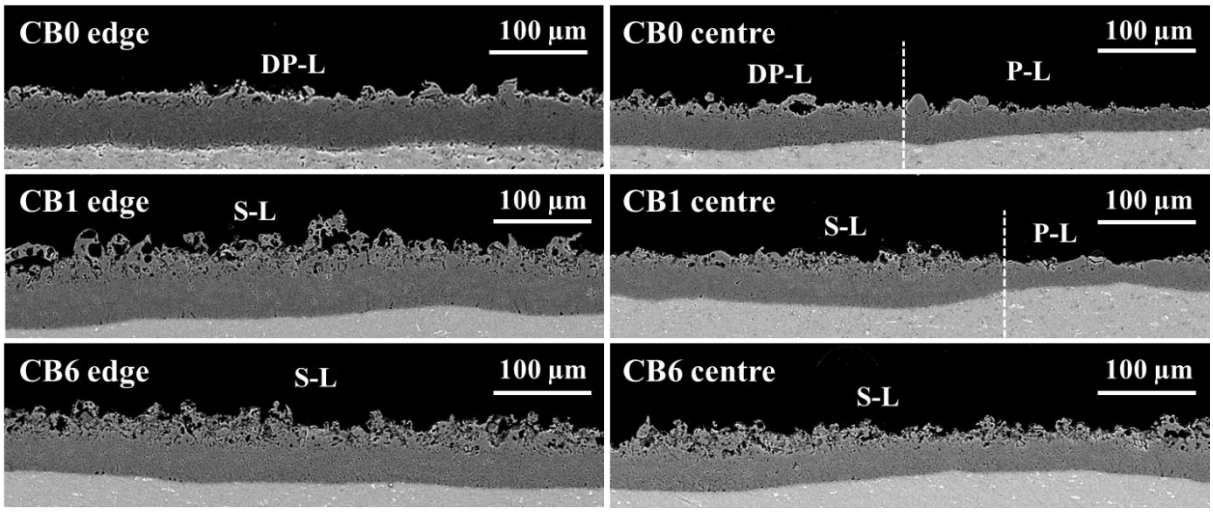

Fig. 8.

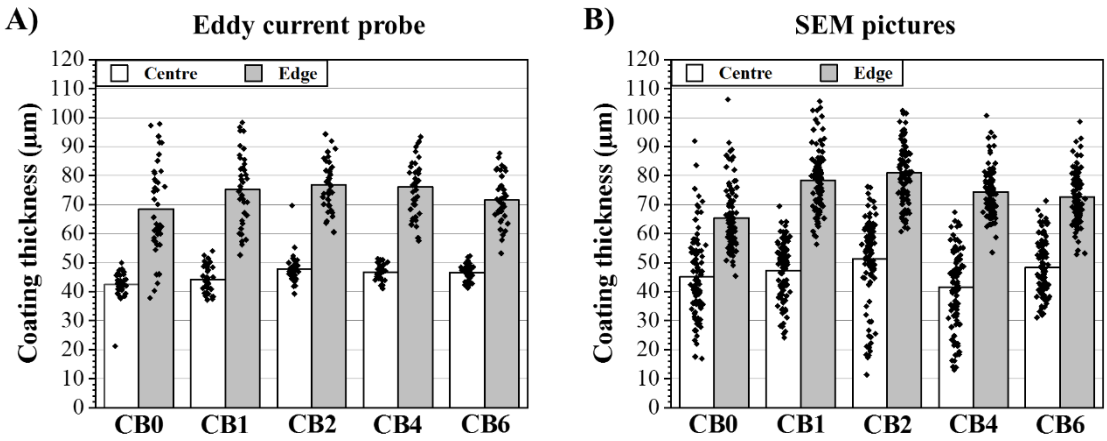

Fig. 9.

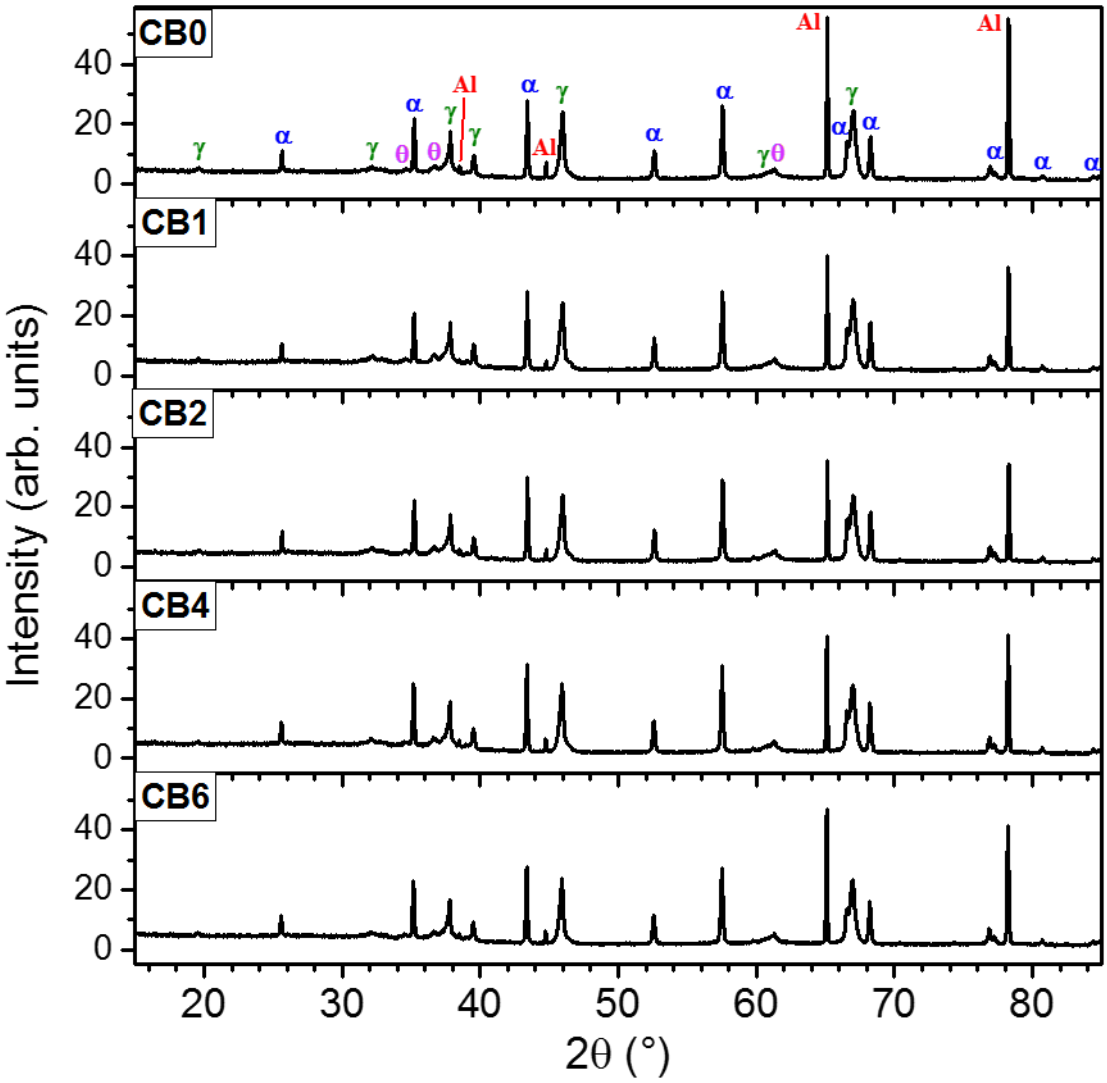

Fig. 10

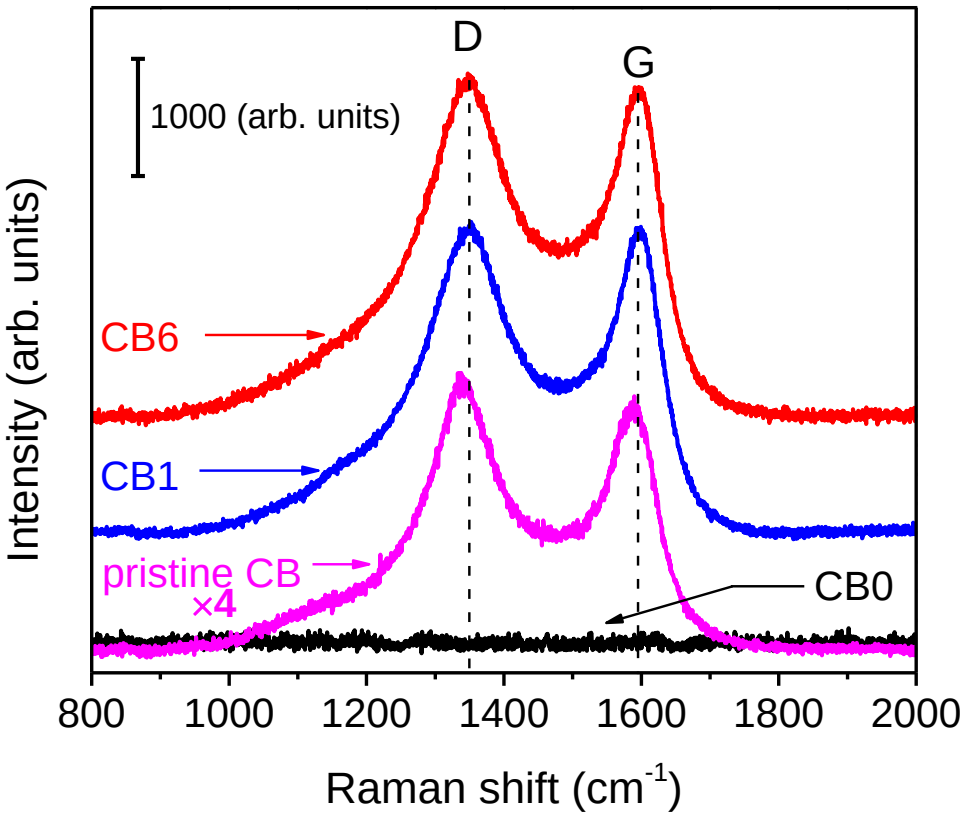

Fig. 11.

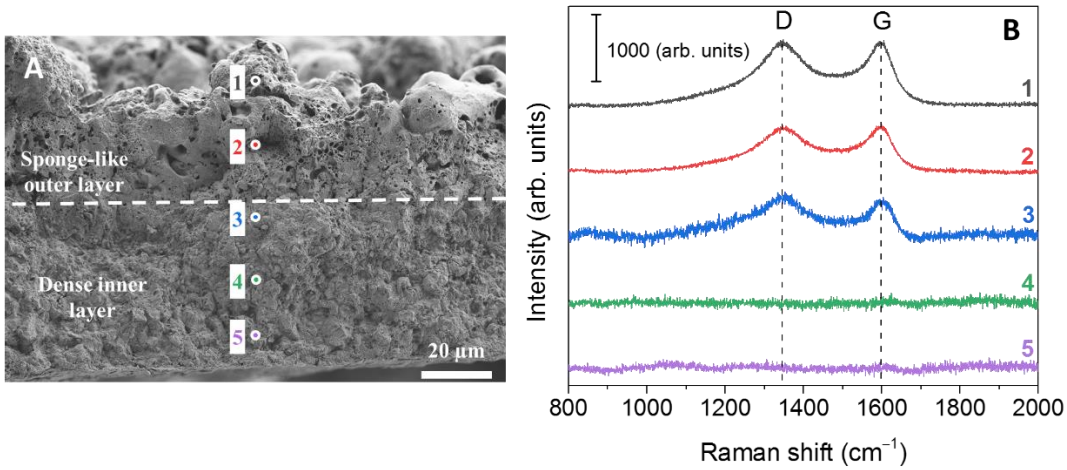

Fig. 12.